ohio2/yla-yla/yla-yla/yla99907/yla5907d07z | xppws | 23:ver.6 | 11/12/08 | 15:14 | Msc: la-2008-02323x | TEID: drh00 | BATID: la1a65

Linear-to-Branched Micelles Transition: A Rheometry and Diffusing Wave Spectroscopy (DWS) Study

C. Oelschlaeger,*,† M. Schopferer,† F. Scheffold,‡ and N. Willenbacher†

Institute of Mechanical Process Engineering and Mechanics, University Karlsruhe, Gotthard-Franz-Str. 3, 76128 Karlsruhe, Germany, and Department of Physics, University of Fribourg, 1700 Fribourg Perolles, Switzerland

Received July 25, 2008. Revised Manuscript Received October 1, 2008

The frequency-dependent shear modulus of aqueous wormlike micellar solutions of cetylpyridinium chloride (CPyCl) and sodium salicylate (NaSal) has been measured over a broad frequency range from 10^{-2} to 10^{6} rad/s using diffusing wave spectroscopy (DWS) based tracer microrheology as well as mechanical techniques including rotational rheometry and oscillatory squeeze flow. Good agreement between mechanical and optical techniques is found in the frequency range from 10^{-1} to 10^{5} rad/s (Willenbacher, N.; Oelschlaeger, C.; Schopferer, M.; Fischer, P.; Cardinaux, F.; Scheffold, F. *Phys. Rev. Lett.* **2007**, *99* (6), 068302). At intermediate frequencies between 10 and 10^{4} rad/s, squeeze flow provides most accurate data and is used to determine the plateau modulus G_0, which is related to the cross-link density or mesh size of the entanglement network, as well as the scission energy E_{sciss}, which is deduced from the temperature dependence of the shear moduli in the plateau zone. In the frequency range above 10^{4} rad/s, DWS including a new inertia correction is most reliable and is used to determine the persistence length l_p. The system CPyCl/NaSal is known to exhibit two maxima in zero-shear viscosity and terminal relaxation time as the salt/surfactant ratio R is varied (Rehage, H.; Hoffman, H. *J. Phys. Chem.* **1988**, *92* (16), 4712−4719). The first maximum is attributed to a transition from linear to branched micelles (Lequeux, F. *Europhys. Lett.* **1992**, *19* (8), 675−681), and the second one is accompanied by a charge reversal due to strongly binding counterions. Here, we discuss the variation of G_0, E_{sciss}, and l_p with salt/surfactant ratio R at constant surfactant concentration of 100 mM CPyCl. G_0 increases at the linear-to-branched micelles transition, and this is attributed to the additional contribution of branching points to the cross-link density. E_{sciss} exhibits two maxima analogous to the zero-shear viscosity, which can be understood in terms of the variation of micellar length and variation of the amount of branched micelles and contour length between branching points consistent with the results of a comprehensive cryo-transmission electron microscopy (TEM) study (Abezgauz, L.; Ramon, O.; Danino, D. Department of Biotechnology and Food Engineering, Technion, Haifa, Israel. European Colloid and Interface Society, Geneva, 2007). The persistence length decreases with increasing R. This decrease is stronger than expected from the decrease of Debye length according to the Odijk−Skolnick−Fixman (OSF) theory and is attributed to the penetration of salicylate ions into the micelles; the linear-to-branched transition obviously does not have an effect on l_p.

1. Introduction

In solution, amphiphilic surfactant molecules can self-assemble to form various structures such as spherical or wormlike micelles, vesicles, or hexagonal and lamellar liquid crystalline structures. These different aggregation structures can show distinct rheological properties. Surfactant solutions with wormlike micellar structures are widely used in home and personal care products as well as enhanced oil recovery but also as drag reduction agents in district heating systems or most recently as templates for asymmetric and aligned nanostructures as well as sieving matrix for separation of DNA fragments.[5,6] The structural and rheological properties of wormlike micelles (WLMs) have been investigated intensively not only because of their wide application range, but also because they show many analogies to covalently bonded polyelectrolytes and can be used as model systems to study the structure and dynamics of polymers. Since micelles break and reform (rate constant k), they are often termed "equilibrium" or "living" polymers. Small changes in surfactant structure, counterion type and concentration, added electrolytes, or temperature can alter the length, flexibility, and interactions of micelles, drastically resulting in pronounced effects on macroscopic rheological properties. In particular, various ionic surfactants show a pronounced maximum of the zero-shear viscosity as the salt/surfactant ratio is varied.[7−11] This is of significant interest from an application point of view, since this viscosity maximum is closely related to the application properties of corresponding surfactant systems, but also from a scientific point of view, since the structural changes corresponding to this viscosity maximum are still not really clear. Several studies support the transition from linear to branched micelles: for example, a combined cryo-transmission electron microscopy (TEM), small-angle neutron scattering (SANS), and rheology study on the system erucyl-bis(hydroxyethyl)methylammonium chloride (EHAC)/KCl consistently revealed a transition from linear to branched micelles around the viscosity maximum.[12] In contrast to ordinary polymers, these branch points can slide along the micelles and hence provide

† University Karlsruhe.
‡ University of Fribourg.

(1) Willenbacher, N.; Oelschlaeger, C.; Schopferer, M.; Fischer, P.; Cardinaux, F.; Scheffold, F. *Phys. Rev. Lett.* **2007**, *99*(6), 068302.
(2) Rehage, H.; Hoffmann, H. *J. Phys. Chem.* **1988**, *92*(16), 4712–4719.
(3) Lequeux, F. *Europhys. Lett.* **1992**, *19*(8), 675–681.
(4) Abezgauz, L.; Ramon, O.; Danino, D. Department of Biotechnology and Food Engineering, Technion, Haifa, Israel. European Colloid and Interface Society, Geneva, 2007.
(5) Walker, L. M. *Curr. Opin. Colloid Interface Sci.* **2001**, *6*(5−6), 451–456.
(6) Yang, J. *Curr. Opin. Colloid Interface Sci.* **2002**, *7*(5−6), 276–281.
(7) Candau, S. J.; Khatory, A.; Lequeux, F.; Kern, F. *J. Phys. IV* **1993**, *3*, 197–209.
(8) Cappelaere, E.; Cressely, R. *Colloid Polym. Sci.* **1998**, *276*, 1050–1056.
(9) Cappelaere, E.; Cressely, R. *Rheol. Acta* **2000**, *39*, 346–353.
(10) Raghavan, S. R.; Kaler, E. W. *Langmuir* **2001**, *17*, 300–306.
(11) Schubert, B. A.; Kaler, E. W.; Wagner, N. J. *Langmuir* **2003**, *19*, 4079–4089.
(12) Croce, V.; Cosgrove, T.; Maitland, G.; Hughes, T.; Karlsson, G. *Langmuir* **2003**, *19*, 8536–8541.

10.1021/la802323x CCC: $40.75

ohio2/yla-yla/yla-yla/yla99907/yla5907d07z | xppws | 23:ver.6 | 11/12/08 | 15:15 | Msc: la-2008-02323x | TEID: drh00 | BATID: la1a65

a high number of degrees of freedom for reptation resulting in the observed viscosity reduction. In contrast, for the system cetyl triammonium chloride (CTAC) and sodium salycilate (NaSal), cryo-TEM images did not reveal significant branching around the viscosity maximum and the viscosity drop was attributed to a change in micellar breakage time.[14] For the systems cetyl triammonium bromide (CTAB)[14,15] and cetyl pyridinium chloride (CPyCl) with NaSal as strongly binding counterion,[2] even a second viscosity maximum is observed when the salt concentration is further increased, but the underlying structural or dynamic change of the system has not been resolved yet. In this study, we use a recently established experimental approach[1] combining mechanical high frequency rheology and optical microrheology to get new insight into structural and dynamic changes accompanying the characteristic viscosity maxima observed in the CPyCl/NaSal system at characteristic surfactant-to-salt ratios R. The newly established approach gives access to the linear viscoelastic properties of these solutions at frequencies up to 1 MHz. We investigate the dependence of the plateau modulus G_0, the scission energy E_{sciss}, and the persistence length l_p with salt/surfactant ratio R at constant surfactant concentration of 100 mM CPyCl. On the one hand, despite the large amount of literature for this system, no results on the scission energy and bending stiffness are available so far. On the other hand, this system is particularly suited for the proposed study, since it has been shown that there is good agreement between mechanical rheometry data and optical microrheology[1,16] in a very broad frequency range, and thus, the high frequency linear viscoelastic properties can be characterized thoroughly.

2. Relationship between Dynamical and Structural Features of Entangled Wormlike Micellar Solutions

Long and flexible linear micelles, commonly referred to as "wormlike" micelles, can be described by a number of structural parameters, which cover a broad range of length scales. The overall length of the micelles is referred to as the contour length L and varies from a few nanometers to micrometers. A mean field treatment of the growth process for highly screened micelles has been obtained from the models derived by Cates[17−19] and predicts an exponential distribution of length $N(L)$:

$$N(L) \propto \exp\left(-\frac{L}{\bar{L}}\right) \tag{1}$$

with the average length given by

$$\bar{L} \cong \varphi^{0.5} \exp\left(\frac{E_{sciss}}{2k_BT}\right) \tag{2}$$

where φ is the surfactant volume fraction, T is the temperature, and E_{sciss} is the scission energy of the micelle, that represents the excess free energy for a pair of hemispherical end-caps relative to a rodlike region containing an equal number of surfactants. Slight changes in the composition of surfactant solutions are expected to affect their overall length, which is directly related to the scission energy. In the present study, we investigate the influence of the scission energy on the dynamics and structure of micellar solutions. For charged systems, this quantity has two contributions:

$$E_{sciss} = E_c - E_e \tag{3}$$

E_c is the energy required to create two hemispherical end-caps as a result of scission of the wormlike micelles and reflects the differences in surfactant packing in the end-caps versus the cylindrical body of the micelles. For nonionic micelles or for ionic micelles at high ionic strength, $E_{sciss} = E_c$. For ionic micelles, repulsion between charged head groups favors micelle breaking and lowers E_{sciss}; this effect is summarized in E_e. According to the theory of Cates and Granek,[57] the scission energy E_{sciss} is related to the temperature dependence of the moduli G' and G'' at intermediate frequencies, in the so-called entanglement regime, where G' exhibits a plateau and G'' ($\ll G'$) goes through a minimum (in so-called Cole−Cole plots, significant deviations occur from the semicircular shape expected for Maxwell fluids). In this regime, the ratio G''_{min}/G_0 is related to l_e (contour length between two successive entanglements) and $\bar{L}$ according to[57]

$$\frac{G''_{min}}{G_0} \sim \frac{l_e}{\bar{L}} \sim \varphi^{-1.85} \exp\left(-\frac{E_{sciss}}{2k_BT}\right) \tag{4}$$

In the case of formation of branched micelles which correspond to the formation of equilibrium cross-links arising through local fusion of micelles, a model based on the coupled reptation/reaction for branched micelles was developed by Lequeux.[3] In the frame of this model, all the results concerning the rheology of linear wormlike micelles can be applied to branched micelles, provided that one substitutes $\bar{L}$ by $\bar{L}_c$, where $\bar{L}_c$ represents the harmonic mean between the average distance from one point along the micelle to the first cross-link and the average distance from that point to the first end-cap. Consequently, we determine the scission energy using the same method (section 4.2.2) for linear as well as for branched micelles. Another key structural parameter for wormlike micellar solutions investigated here is the plateau modulus G_0. This parameter, determined at intermediate frequencies, is directly related to the mesh size ξ of the system with $G_0 \sim \xi^{-3}$ and is typically independent of temperature.[1] We also investigate the high frequency range; in this regime, the stress relaxation, for linear micelles as well as for branched micelles, is controlled by the internal dynamics of short micelle segments and the moduli G' and G'' show characteristic scaling behavior.

$$G' \sim G'' \sim \omega^{\alpha} \tag{5}$$

First, the Rouse−Zimm modes dominate and $\alpha = 1/2 - 2/3$.

At even higher frequencies, internal bending modes of single Kuhn segments determine G' and G'', and hence, these dynamic parameters are related to the bending modulus κ as a structural parameter; κ is often expressed in terms of the persistence length $\kappa = k_BT/l_p$. In this frequency range, the scaling exponent $\alpha = 3/4$ as predicted by Morse,[20] and Gittes and MacKintosh.[21]

The transition between these scaling regimes is marked by the inverse of the shortest Rouse relaxation time $\omega_0 = \tau_0^{-1}$ which is directly related to the persistence length l_p.

$$\omega_0 = \frac{k_BT}{8\eta_s l_p^3} \tag{6}$$

where η_s is the solvent viscosity.

(13) Clausen, T.; Vinson, P. K.; Minter, J. R.; Davis, H. T.; Talmon, Y.; Miller, W. G. *J. Phys. Chem.* **1992**, *96*(1), 474–484.
(14) Nemoto, N.; Kuwahara, M.; Yao, M.-L.; Osaki, K. *Langmuir* **1995**, *11*, 30–36.
(15) Galvan-Miyoshi, J.; Delgado, J.; Castillo, R. *Eur. Phys. J. E.* **2008**, *26*(4), 369–377.
(16) Buchanan, M.; Atakhorrami, M.; Palierne, J. F.; Schmidt, C. F. *Macromolecules* **2005**, *38*, 8840–8844.
(17) Cates, M. E. *J. Phys. (Paris)* **1988**, *49*, 1593.
(18) Cates, M. E. *Macromolecules* **1987**, *20*, 2289.
(19) Israelachvili, J.; Mitchell, D. J.; Ninham, B. W. *J. Chem. Soc., Faraday Trans. 2* **1976**, *72*, 1525.
(20) Morse, D. C. *Phys. Rev. E* **1998**, *58*(2), R1237–R1240.
(21) Gittes, F.; MacKintosh, F. C. *Phys. Rev. E* **1998**, *58*(2), R1241–R1244.

The persistence length l_p can also be determined from the absolute values of G' and G'' in the $\alpha = 3/4$ scaling regime according to a relationship based on a statistical mechanical treatment of the single filament stress response of semiflexible chains presented in ref 21:

$$G^* = \frac{\rho}{15} K l_p \left(\frac{-2i\xi}{K}\right) \omega^{\frac{3}{4}} - i\omega\eta_s \qquad (7)$$

where ζ is the lateral drag coefficient and ρ is the area density of micelles. The latter can be calculated as $\rho = \phi_{surf}/((\pi/4)d_{mic}^2)$ where ϕ_{surf} is the surfactant concentration (vol/vol) and $(\pi/4)d_{mic}^2$ is the cross-sectional area of the micelles. So far, l_p has been determined using various scattering techniques including small-angle neutron scattering (SANS)[22−24] as well as static and dynamic light scattering.[14,25−27] Birefringence measurements can also be used to determine l_p.[28] Recently, it has been demonstrated that also another neutron scattering technique, namely, neutron spin echo (NSE), can be used to determine the persistence length.[29] Robust and reliable models are available to analyze scattering data, and SANS is a well established tool to characterize wormlike micelles. However, limited access to large scale facilities hinders its broad application for systematic investigations with careful parameter variation. Light scattering techniques are suitable for stiff micelles ($l_p \approx 100$ nm) only, due to the different q-range which is accessed. Birefringence measurements require the knowledge of optical constants which are often not known. Recently, we have demonstrated that the high frequency range where the $\omega^{3/4}$-scaling occurs can be accessed by optical as well as mechanical rheometry. Accordingly, these techniques can be used to determine l_p according to eqs 5 and 6 even for l_p values down to a few nm.[1] In order to improve the quality of the DWS data and to increase the accessible frequency range to the MHz range, a self-consistent inertia correction has been introduced[1,30−32] for the DWS data.

All these structural features, the characteristic length scales, and the corresponding characteristic relaxation times strongly depend not only on the chemical nature and concentration of the surfactant or surfactant mixture under consideration, but also on the nature and concentration of the counterion (binding vs nonbinding) and the ionic strength of the solution. This has been studied intensively not only by rheological experiments but also by using electron microscopy and various scattering techniques.[11,28,33,34] Cryo-TEM, for example, has been used to visualize entanglements, branching, and the semiflexible, wormlike nature of the micelles directly.[12,13,35−37]

In the first part of this paper, we establish the relationship between dynamical and structural features of entangled solutions of wormlike micelles and we compare results from mechanical rheometry and optical microrheology. We focus on three different parameters: plateau modulus, scission energy, and persistence length. In the second part of the paper, we investigate the effect of salt concentration on these three parameters for the system CPyCl in the presence of NaSal.

3. Materials and Methods

3.1. Sample Characteristics. Aqueous solutions of surfactant/counterion mixtures cetylpyridinium chloride/sodium salicylate (CPyCl/NaSal) were used as model systems. CPyCl and NaSal were both obtained from C. Roth. The sample solutions were prepared by gently stirring the surfactant and salt in deionized water. For equilibrium measurements, they were stored for at least 1 day at 20 °C. This solution exhibits a very strong viscoelastic response in the temperature range between 20 and 40 °C.[38,39]

3.2. DWS Based Optical Microrheology. The basic idea of optical microrheology is to study the equilibrium thermal response of small (colloidal) particles embedded in a material and thereby obtain quantitative information about the macroscopic loss and storage moduli, $G'(\omega)$ and $G''(\omega)$, over an extended range of frequencies. The modern way of using this technique was introduced in the mid-1990s when Mason and Weitz proposed a quantitative relation between the tracer mean-squared displacement $\langle\Delta r^2(t)\rangle$ and the complex shear modulus $G^*(\omega)$.[40] The Laplace transform of the particle mean squared displacement $\langle\Delta\tilde{r}^2(i\omega)\rangle$ is related to the complex modulus of the sample via a generalized Stokes−Einstein equation (GSE):

$$G^*(\omega) = \frac{k_B T}{\pi a i\omega \langle\Delta\tilde{r}^2(i\omega)\rangle} = G'(\omega) + iG''(\omega) \qquad (8)$$

Assuming that the complex fluid can be treated as an isotropic, incompressible continuum around a sphere, this relation was later confirmed theoretically.[41] Under this condition, the GSE is valid essentially for all cases of practical interest except for the limit of ultrahigh frequencies where inertia effects start to play a role. At times much shorter than 10^{-5} s, or frequencies well above $\omega = 10^5$ rad/s, inertia effects become significant.[30] This means that $\langle\Delta r^2(t)\rangle$ not only is given by the viscous (or viscoelastic) properties of the medium as assumed above but is distorted by inertia effects at times much shorter than 10^{-4} s. The goal is therefore to recover the motion pattern one would observe in the absence of inertia effects. In order to be able to access this interesting ultrahigh frequency regime, we have recently introduced a simple (self-consistent) correction scheme.[1] Previous studies on dense colloidal suspensions have shown that the effective high frequency viscosity determines the influence of fluid inertia.[31] From the raw $G''(\omega)$ data, we determine the effective high frequency viscosity of approximately 3 mPas from a fit to the loss modulus $G''(\omega) = \eta(\omega)\omega$ in the regime $\omega = 10^5 - 10^6$ s^{-1}. We then correct the particle mean square displacement for inertia effects based on the theory of Hinch[32] developed for the motion of a sphere in a simple fluid with viscosity η. In a second iteration step, we again fit the resulting loss modulus and repeat this procedure several times. In our case, the correction factor attains its smallest value of 0.7 for the shortest time analyzed $\tau = 5 \times 10^{-7}$ s.

For a quantitative interpretation of the raw experimental data $\langle\Delta r^2(t)\rangle$, the Laplace transformation is the most critical part of the analysis. To reduce truncation errors, we apply a procedure suggested by Mason and co-workers. We estimate $\tilde{G}(s)$ by substituting $\langle\Delta r^2(t)\rangle$ into an algebraic Stokes−Einstein form:[42]

(22) Magid, L. J.; Han, Z.; Li, Z.; Butler, P. D. *J. Phys. Chem. B* **2000**, *104*(29), 6717–6727.
(23) Hoffmann, H.; Kalus, J.; Schwandner, B. *Ber. Bunsen−Ges.* **1987**, *91*, 99–106.
(24) Pedersen, J. S.; Laso, M.; Schurtenberger, P. *Phys. Rev. E* **1996**, *54*, R5917–5920.
(25) Brown, W.; Johansson, K.; Almgren, M. *J. Phys. Chem.* **1989**, *93*(15), 5888–5894.
(26) Imae, T. *J. Phys. Chem.* **1990**, *94*, 5953–5959.
(27) Buhler, E.; Munch, J. P.; Candau, S. J. *J. Phys. II* **1995**, *5*(6), 765–787.
(28) Shikata, T.; Dahman, S. J.; Pearson, D. S. *Langmuir* **1994**, *10*(10), 3470–3476.
(29) Nettesheim, F.; Wagner, N. J. *Langmuir* **2007**, *23*, 5267–5269.
(30) Weitz, D. A.; Pine, D. J.; Pusey, P. N.; Though, R. J. A. *Phys. Rev. Lett.* **1989**, *63*, 1747.
(31) Ladd, A. J. C.; Gang, H.; Zhu, J. X.; Weitz, D. A. *Phys. Rev. Lett.* **1995**, *74*, 318.
(32) Hinch, E. *J. Fluid Mech.* **1975**, *72*, 499.
(33) Cates, M. E.; Candau, S. J. *J. Phys.: Condens. Matter* **1990**, *2*, 6869–6892.
(34) Magid, L. J.; Li, Z.; Butler, P. D. *Langmuir* **2000**, *16*, 10028–10036.
(35) Lin, Z. *Langmuir* **1996**, *12*(7), 1729–1737.
(36) Bernheim-Groswasser, A.; Wachtel, E.; Talmon, Y. *Langmuir* **2000**, *16*(9), 4131–4140.
(37) Bernheim-Groswasser, A.; Zana, R.; Talmon, Y. *J. Phys. Chem. B* **2000**, *104*(51), 12192–12201.
(38) Rehage, H.; Hoffmann, H. *Mol. Phys.* **1991**, *74*, 933.
(39) Fischer, P.; Rehage, H. *Rheol. Acta* **1997**, *36*, 13.
(40) Mason, T. G.; Weitz, D. A. *Phys. Rev. Lett.* **1995**, *74*, 1250.
(41) Levine, A. J.; Lubensky, T. C. *Phys. Rev. E.* **2001**, *63*, 1–4.

$$\tilde{G}(s) = \frac{k_B T}{\pi a \langle \Delta r^2(t) \rangle \Gamma[1 + (\partial \ln \langle \Delta r^2(t) \rangle / \partial t)^{t=1/s}} \quad (9)$$

In order to reduce scatter, we first fit $\langle \Delta r^2(t) \rangle$ with a polynomial of order 6 or 7 and then use eq 9 to extract the moduli $G'(\omega)$ and $G''(\omega)$. We have checked that the choice of the polynomial order and the range of data selected do not influence the results. Finally, it is worthwhile to note that, contrary to mechanical measurements, the in- and out-of-phase contributions are not measured independently but have to be extracted from a single value of the slope $\partial \ln \langle \Delta r^2(t) \rangle / \partial t$. As a consequence, if $G'(\omega)$ and $G''(\omega)$ are of different magnitude, the lower value extracted from DWS measurements is often not very well defined.

A number of methods have been applied successfully to measure the particle mean square displacement, notably single particle tracking by microscopy, laser deflection, and diffusing wave spectroscopy (DWS).[43−45] In this work, we have chosen DWS as the only technique that provides access to frequencies well above 10^4 rad/s. The DWS technique is an extension of dynamic light scattering (DLS) to soft materials exhibiting strong multiple scattering.[46] The method allows one to monitor the displacement of micrometer sized colloidal particles with subnanometer precision and on time scales as short as 10 ns. In recent years, significant progress has been made in development of the DWS approach, and it has been successfully applied to the study of fluid and solid media, for example, colloidal suspensions, gels, and biocolloids (yogurt and cheese) as well as ceramic slurries and green bodies.[47−50] In a DWS experiment, coherent laser light impinges on one side of a turbid sample and the intensity fluctuations of the light propagated through the sample are then analyzed either in transmission or backscattering geometry. A diffusion model is used to describe the propagation of photons across the sample. Analogous to traditional dynamic light scattering (DLS), for the case of noninteracting particles, it is possible to express the measured intensity autocorrelation function (ICF) $g_2(\tau) - 1 = \langle I(t) I(t+\tau) \rangle / \langle I \rangle^2 - 1$ in terms of the mean square displacement of the scattering particle,

$$g_2(\tau) - 1 = \left[\int_0^\infty \mathrm{d}s \, P(s) \exp(-(s/l^*) k^2 \langle \Delta r^2(\tau) \rangle \right)^2 \quad (10)$$

with $k = 2\pi n/\lambda$ being the wavenumber of light in a medium with refractive index n. $P(s)$ is the distribution of photon trajectories of length s in the sample, and it can be calculated within the diffusion model taking into account the experimental geometry. For the case of transmission through a slab (plane-wave illumination), one obtains

$$g_2(t) - 1 = \left[\frac{(L/l^* + 4/3) \left\langle \sqrt{k_0^2 \Delta r^2(t)} \right\rangle}{\sinh\left[(L/l^* + 4/3) \left\langle \sqrt{k_0^2 \Delta r^2(t)} \right\rangle \right]} \right]^2 \quad (11)$$

The transport mean free path l^* characterizes the typical step length of the photon random walk, given by the individual particle scattering properties and particle concentration, and l^* can be determined independently by a comparison of the measured count rate to the one obtained with a sample of known l^* (ref 51) and therefore enters the analysis as a constant parameter. Equation 11 numerically calculated the particle mean square displacement $\langle \Delta r^2(t) \rangle$ from the measured autocorrelation function $g_2(t)$. In our experiments, we added 2% polystyrene sulfonate particles (diameter 720 nm, IDC Corporation, Portland, OR) to the micellar solution temporarily heated to 60 °C in order to reduce the viscosity. The sample was filled in standard glass cuvettes (Hellma) with a path length of 2 mm and a width of 10 mm. The temperature was controlled within ±0.1 °C using a home-built temperature control chamber. A frequency doubled neodymium:yttrium vanadate (Nd:YV04) laser (Verdi, Coherent) operating at a wavelength $l = 532$ nm was used to illuminate a circular ground glass mounted on a two phase stepper motor (KH42HM2-851 from Japan Servo). Putting a fast rotating diffuser in the optical path between the laser and sample allows for more efficient ensemble averaging.[52] We collected the transmitted light coming from the ground glass and focused it onto the sample with a spot size diameter of roughly 5 mm. The scattered laser light was then collected using a single-mode optical fiber and single photon counter and subsequently analyzed by using a digital correlator (Correlator.com, NJ). By numerical analysis using eq 11, we extracted the particle mean square displacement $\langle \Delta r^2(t) \rangle$ from the ICF typically over a range of values $g_2 = 0.01-0.99$. Figure 1shows a schematic diagram of our DWS setup.

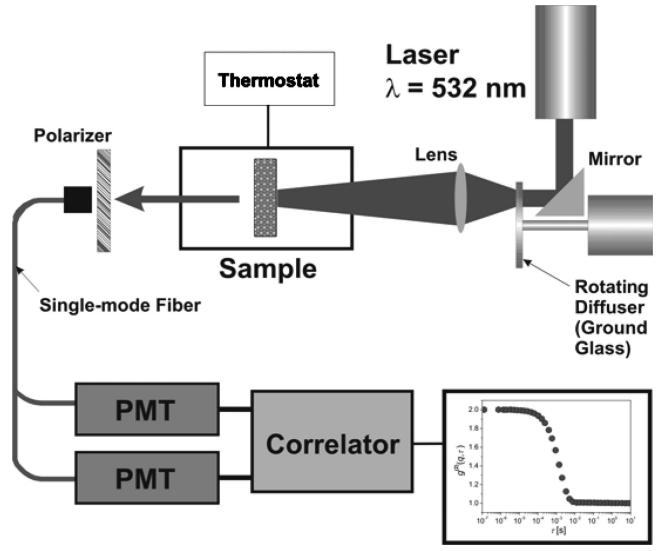

Figure 1. Schematic diagram of our DWS setup. Laser light is scattered from a ground glass rotated by a fast stepper motor, and the transmitted light is collected by a lens to illuminate the sample. A single mode fiber collects the scattered light in transmission. The collected light is subsequently analyzed by a single-photon detector and digital photon counter.

3.3. Squeeze Flow. Oscillatory squeeze flow experiments were performed using a piezo-driven axial vibrator (PAV). General theory of squeeze flow is covered in standard textbooks of fluid mechanics.[53] The theory of the PAV as well as the mechanical and electronic setup are thoroughly discussed elsewhere,[54,55] and therefore, this is summarized here only briefly. The actor is a thin-walled quadratic copper tube with a thick stainless steel plate on top. Four piezoelectric actuators are attached to two opposite walls of the tube in order to exert the vibrations, and four additional piezoelectric sensors are fixed to the remaining sides in order to pick up the response signal. Direct coupling of excitation and detection is avoided by four partial cuts of the tube parallel to the longitudinal axis. This lower part of the device is surrounded by a double-walled cylinder allowing for circulation of a thermostatting fluid, and the temperature is controlled

(42) von Berlepsch, H.; Harnau, L.; Reineker, P. *J. Phys. Chem. B* **1998**, *102*, 7518.
(43) Xu, J.; Tseng, Y.; Carriere, C. J.; Wirtz, D. *Biomacromolecules* **2002**, *3*, 92–99.
(44) Mason, T. G.; Ganesan, K.; van Zanten, J. H.; Wirtz, D.; Kuo, S. C. *Phys. Rev. Lett.* **1997**, *79*, 3282–3285.
(45) Gardel, M. L.; Valentine, M. T.; Crocker, J. C.; Bausch, A. R.; Weitz, D. A. *Phys. Rev. Lett.* **2003**, *91*, 158302.
(46) Maret, G.; Wolf, P. E. *Z. Phys. B: Condens. Matter* **1987**, *65*, 409–413.
(47) Zakharov, P.; Cardinaux, F.; Scheffold, F. *Phys. Rev. E* **2006**, *73*, xxx.
(48) Scheffold, F.; Schurtenberger, P. *Soft Mater.* **2003**, *1*, 139.
(49) Schurtenberger, P.; Stradner, A.; Romer, S.; Urban, C.; Scheffold, F. *CHIMIA: Int. J. Chem.* **2001**, *55*(3), 155–159.
(50) Heinemann, C.; Cardinaux, F.; Scheffold, F.; Schurtenberger, P.; Escher, F.; Conde-Petit, B. *Carbohydr. Polym.* **2004**, *55*(2), 155–161.
(51) Kaplan, P. D.; Kao, M. H.; Yodh, A. G.; Pine, D. J. *Appl. Opt.* **1993**, *32*, 3828.
(52) Zakharov, P.; Cardinaux, F.; Scheffold, F. *Phys. Rev. E.* **2006**, *73*, 011413.
(53) Bird, R. B.; Armstrong, R. C.; Hassager, C. *Dynamics of Polymeric Liquids, Vol. 1, Fluid Dynamics*, 2nd ed.; Wiley: New York, 1987.
(54) Crassous, J. J.; Regisser, R.; Ballauff, M.; Willenbacher, N. *J. Rheol.* **2005**, *49*, 851.
(55) Kirschenmann, L. Ph.D. Thesis, Universität Ulm, 2003, p 11.

with an accuracy of ±0.04 °C. The whole setup is covered by a thick metal lid, which is the upper boundary of the gap and provides a complete sealing for the apparatus. The instrument is operated by a lock-in amplifier. The applied voltage of the driving piezos is proportional to the axial force. The instrument operates at a constant force amplitude F_0, and from the complex ratio of the dynamic displacement of the lower plate (amplitude ≈ 5 nm) with and without fluid $xf^*/x0^*$ one can calculate the complex squeeze stiffness K^* of the fluid using an appropriate mechanical equivalent circuit and solving its equations of motion. In order to calculate K^* from the ratio of the output voltage $U/U0$ and the phase difference $\Delta\varphi$ recorded by the lock-in amplifier with and without fluid, the mechanical properties (spring constant mass, resonance frequency) of the instrument itself have to be determined as described in ref 55. Finally, K^* is related to the complex shear modulus G^* and compressibility k_c^* by[55]

$$\frac{1}{K^*} = \frac{2d^3}{3\pi R^4}\left(\frac{1}{G^*} + \frac{3R^2}{2d^2}k_c^*\right) \qquad (12)$$

where R (here 10 mm) is the radius and d is the height of the gap. The determination of G^* strongly depends on the exact knowledge of d, which is determined by calibration using Newtonian liquids with viscosities between 1 and 2000 mPas. Gap heights between 15 and 100 μm have been used here. The required sample volume is on the order of 100 μL depending on the height of the gap. Samples have to be degassed carefully in order to avoid artificial compressibility from entrapped air. In principle, the measured G^* values have to be corrected for the k_c^* contribution. For viscoelastic surfactant solutions investigated, here G^* is typically far below 1000 Pa and the compressibility is approximately that of water ($k_{c,w} = 4.6 \times 10^{-10}$ Pa^{-1} at 20 °C). Therefore, the corresponding correction to G^* is well below 5% and can thus be safely neglected. Dynamic shear moduli G^* in the range from 0.1 Pa to 10 kPa are accessible.

3.4. Rotational Rheometry. A rotational rheometer Thermo MARS II equipped with a cone-plate measuring cell (diameter d_{CP} = 35 mm, cone angle $\alpha_{cone} = 4°$) was used to perform small amplitude oscillatory shear experiments covering the frequency range from 0.01 to 100 rad/s at a strain amplitude $\gamma_0 = 0.1$. Strain sweep experiments performed prior to the frequency sweeps confirm that this strain amplitude is sufficiently small to provide a linear material response at all investigated frequencies. Measurements were performed at temperatures between 20 and 40 °C. A solvent trap was used to avoid evaporation of the sample during the experiment.

4. Results and Discussion

4.1. Comparison of Mechanical Rheometry and DWS Measurements. The variation of the dynamic shear moduli G' and G'' as a function of frequency as determined from mechanical and optical rheometry has been investigated for the system CPyCl/NaSal at $0.5 < R < 5$. In general, good agreement is found between mechanical and optical methods. Results for $R = 0.6$, corresponding to the first viscosity maximum, have been reported earlier.[1] The shapes of the relaxation spectra from DWS and mechanical rheometry coincide very well over the whole frequency range, but the DWS absolute values of G' and G'' are shifted with respect to the mechanical measurements. The reasons for this shift have already been discussed in ref 1; they can been attributed to uncertainties in experiment as well as residual perturbations of the complex fluid in the particle vicinity[56] as discussed below. Variations of the zero-shear viscosity η_0, the terminal relaxation time T_R, and the plateau modulus G_0 as a function of R from mechanical and optical techniques are given in Figure 2. T_R and G_0 are directly deduced from the modulus curves. T_R is given by the inverse angular frequency corresponding the first crossover between G' and G''. For DWS and oscillatory squeeze flow, G_0 is determined as the value of the modulus G' at the frequency at which G'' has its local minimum, $G\min''$. For rotational rheometry, $G0$ is taken as the value of G' where it exhibits a constant plateau, since the minimum in G'' is not accessible with this technique. The zero-shear viscosity is obtained by using the equation $\eta 0 \approx G0T\mathrm{R}$. The first observation is that the variations of $\eta 0$, $T\mathrm{R}$, and $G0$ as a function of R are qualitatively the same values independent of the technique used. Both $\eta 0$ and $T\mathrm{R}$ pass through two maxima:[2] the first maximum occurs at $R \sim 0.65$ and the second at $R \sim 3$. Interpretations of these variations will be discussed below. For $T\mathrm{R}$, the absolute values are in very good agreement for the different techniques, and the differences are within the experimental error. Concerning the variation of the plateau modulus, the results obtained by rotational rheometry and oscillatory squeeze flow are in good agreement at all salt concentrations investigated. On the contrary, the values of $G0$ deduced from DWS measurements show strong deviations (factor 1.5 up to 4.5) from mechanical results in a range of $0.7 < R < 1.4$. A similar result was obtained by Galvan-Miyoshi et al.[15] studying the micellar CTAB/NaSal system. They also compared DWS results with those obtained from mechanical rheometry and found differences between $G0$ values increasing with an increase of salicylate concentration. They speculate that large quantities of free ions (Sal^-) in solution are responsible for this behavior. The free ions are not incorporated into the micelles and could therefore modify the mobility of the Brownian particles. This explanation is not valid in our case, because deviations occur at intermediate R values ($0.7 < R < 1.4$) and not at the highest R values. Alternatively, tracer sedimentation was considered to be responsible for these deviations. In that case, the tracer concentration should increase toward the bottom of the cell, and as a consequence the transport mean free path l^* would be underestimated and accordingly G' and G'' would be overestimated. This hypothesis can be rejected, because experimentally all l^* values are around a constant value of 200 ± 30 μm and such differences could not explain a shift factor of 4.5 in the plateau modulus. The compatibility of the tracers and the surrounding medium can be shown by measuring samples with and without tracers mechanically, and we find no measurable

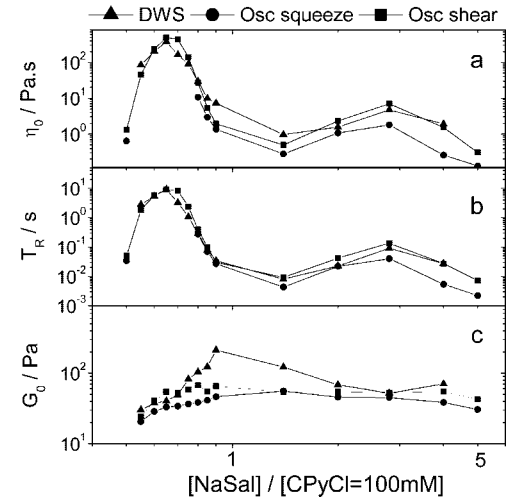

Figure 2. Zero-shear viscosity η_0 (a), terminal relaxation time T_R (b), and plateau modulus G_0 (c) as a function of R = [NaSal]/[CPyCl] at constant surfactant concentration of 100 mM CPyCl obtained from DWS (triangles), oszillatory squeeze flow (circles), and rotational rheometry (squares). T = 20 °C. All the error bars are as large as the size of the different symbols.

(56) Chen, D. T.; Weeks, E. R.; Crocker, J. C.; Islam, M. F.; Verma, R.; Gruber, J.; Levine, A. J.; Lubensky, T. C.; Yodh, A. G. *Phys. Rev. Lett.* **2003**, *90*, 108301.

ohio2/yla-yla/yla-yla/yla99907/yla5907d07z | xppws | 23:ver.6 | 11/12/08 | 15:15 | Msc: la-2008-02323x | TEID: drh00 | BATID: la1a65

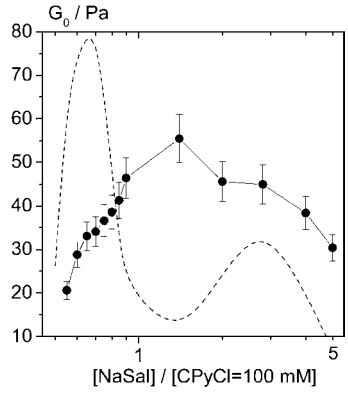

Figure 3. Plateau modulus G_0 (circles) as a function of R obtained from oszillatory squeeze flow measurements at $T = 20$ °C. The dashed line represents the variation of the zero-shear viscosity η_0 in an arbitrary unit.

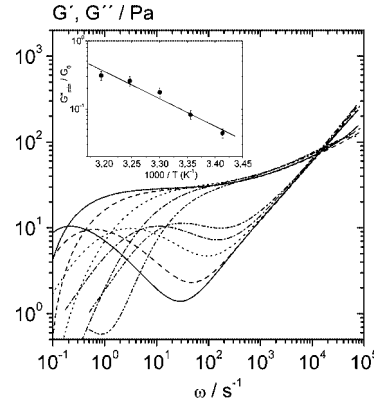

Figure 4. Dynamic shear moduli G' and G'' of an aqueous solution of 100 mM CPyCl/60 mM NaSal as a function of temperature obtained from DWS measurements: 20 °C (solid line), 25 °C (dashed line), 30 °C (dotted line), 35 °C (dash-dotted line), 40 °C (dash-dotted-dotted line). Inset: Ratio of the minimum value of G'' and the plateau modulus G_0 as a function of $1/T$ for the same solution.

differences within experimental errors. Nevertheless, this not to exclude that a small fraction of surfactant may adsorb at the surface of the tracer particles and therefore modify their mobility. Such an adsorption may have no effect on mechanical measurements but on DWS results. Aggregation of tracer particles or a local structure formation hindering tracer motion may be other possible scenarios which would reduce the plateau value of the mean square displacement and thus result in an apparent increase of G_0. We have no indication for heterogeneity of the solutions investigated here, since they are all transparent and monophasic at $T = 20$ °C. Aggregation seems to be an issue; we have observed significant particle aggregation in aqueous suspensions by visual inspection in an optical microscope at least for large tracer particles (2.3 μm diameter), and typically these aggregates consisted of 2−3 particles. Finally, we have performed DWS measurements on the system for $R = 0.9$, for which G_0 deviates the most from mechanical data, using tracers with a larger diameter of 1.3 μm. The shape of the curve is similar to that obtained with the 0.72 μm tracer diameter, but the plateau modulus has decreased from 211 to 100 Pa. This value is still 2 times higher than the mechanical value (50 Pa), but it seems that the diameter of the tracer particle may have some effect on the DWS measurements. Particle aggregation as well as adsorption of surfactant on the tracer surface is expected to depend on surfactant concentration, ionic strength, as well as particle size and concentration. This phenomenon is currently under investigation.

4.2. Effect of Salt on Structural and Dynamic Properties. *4.2.1. Plateau Modulus.* Almost all of the literature dealing with the linear viscoelastic properties of wormlike micelles are based on data from small amplitude oscillatory shear experiments performed by conventional rotational rheometry and are thus limited to the frequency range $\omega < 100$ rad/s. In order to provide the most accurate data at intermediate frequencies between 10 and 10^4 rad/s, we used oscillatory squeeze flow measurement to determine the plateau modulus G_0, which is related to the cross-link density or mesh size of the entanglement network. In Figure 3, we give the variation of the plateau modulus as a function of the ionic strength for the system CPyCl/NaSal at a constant surfactant concentration of 100 mM. The shear modulus varies significantly with ionic strength. It increases by approximately a factor of 2 from $R = 0.5$ to 1.4, with the range corresponding to the first zero-shear viscosity maximum, and then slightly decreases up to $R = 5$. Cryo-TEM pictures taken for the same salt/surfactant system, but at a surfactant concentration of 15 mM, clearly show a transition from linear to branched micelles at the first maximum of zero-shear viscosity, with the branching density increasing up to the minimum of η_0.[4] The increase in G_0 can thus be attributed to the additional contribution of branching points to the cross-link density. In a previous study performed at a surfactant concentration of 60 mM,[2] G_0 was found to be independent of salt concentration. One possible explanation of this contradictory observation is that, with 60 mM CPyCl, the amplitude of the two zero-shear viscosity maxima is about a factor of 10 lower compared to the system with 100 mM CPyCl. Accordingly, the contribution of branching points to G_0 is lower and presumably within experimental uncertainty. The slight decrease of G_0 for $R > 1.4$ can at least qualitatively be attributed to a decrease of the branching density accompanied by an increase of micelle length as shown by the cryo-TEM images taken for R values in the region of the second η_0 increase. Furthermore, TEM images for samples with R values corresponding to the second η_0 maximum show a shortening of the micelles and an increase of the branching density, but also the formation of micellar rings is observed. The formation of branching seems not to compensate the formation of micellar rings, since G_0 further decreases.

4.2.2. Scission Energy of Wormlike Micelles. E_{sciss} is calculated from the temperature dependence of the ratio $G\text{min}''/G0$ according to eq 4. The frequency range of oscillatory shear rheometry is not always sufficient to determine this minimum correctly, but mechanical squeeze flow gives reliable values for $G\text{min}''/G0$ and thus allows for an accurate determination of the scission energy. Figure 4 shows the relaxation spectra from DWS measurements for the system with $R = 0.6$ at four different temperatures between 20 and 40 °C. The terminal zone and the Maxwell relaxation frequency ωr are strongly shifted at higher frequencies, and the absolute value of G'' around its minimum at intermediate frequencies strongly increases as temperature is raised. This directly shows that the micellar contour length $\bar{L}$ decreases as temperature goes up. The plateau modulus, $G0$, is almost independent of temperature, which means that the mesh size ξ of the entanglement network is essentially independent of temperature, irrespective of the drastic change in $\bar{L}$. The insert of Figure 4 represents the variation of $G\text{min}''/G0$ with $1/T$. Esciss can be extracted from the slope of this semilogarithmic plot of $G\text{min}''/G0$ versus $1/T$. The variation of Esciss as a function of salt concentration is shown in Figure 5, where values extracted from DWS and oscillatory squeeze flow are compared. For both

(57) Granek, R.; Cates, M. E. *J. Chem. Phys.* **1992**, *96*, 4758.

ohio2/yla-yla/yla-yla/yla99907/yla5907d07z | xppws | 23:ver.6 | 11/12/08 | 15:15 | Msc: la-2008-02323x | TEID: drh00 | BATID: la1a65

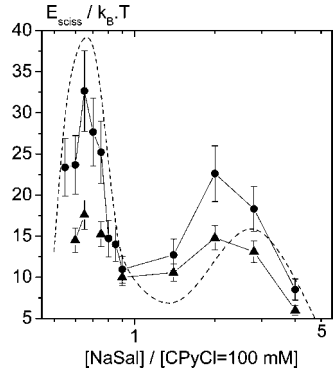

Figure 5. Dependence of scission energy E_{sciss} as a function of R obtained from DWS (circles) and oszillatory squeeze flow (triangles) measurements. The dashed line represents the variation of the zero-shear viscosity η_0 in an arbitrary unit.

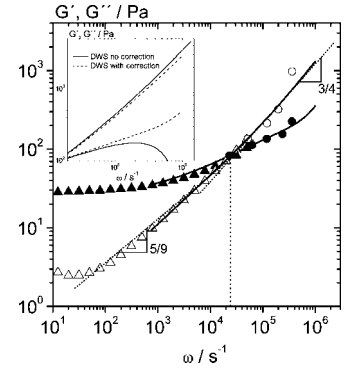

Figure 6. Dynamic shear moduli G' and G'' of an aqueous solution of 100 mM CPyCl/60 mM NaSal at $T = 20$ °C obtained from DWS (solid lines) and various mechanical rheometers (G', solid symbols; G'', open symbols): oszillatory squeeze flow (triangles) and torsional resonators from ref 1 (circles). Inset: G', G'' after inertial correction (dotted lines) of the DWS raw data (solid lines).

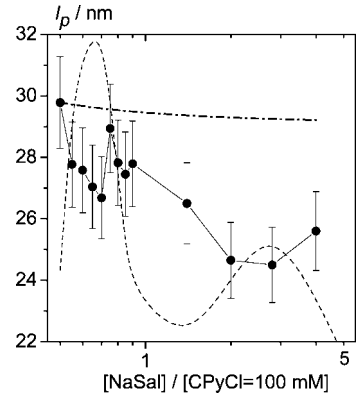

Figure 7. Dependence of persistence length l_p from DWS measurements (circles, 5% error bars) and from OSF theory normalized to the DWS l_p value at $R = 0.5$ (dash-dotted line) as a function of R. The dashed line represents the variation of the zero-shear viscosity η_0 in an arbitrary unit.

techniques, E_{sciss} exhibits two maxima analogous to the variation of the zero-shear viscosity. The first increase in E_{sciss} directly reveals the increase of the average length of the linear micelles, which is due to the increasing screening of the electrostatic repulsions between the charged head groups. This results in a reduction of the optimal molecular area at the hydrocarbon−water interface, leading to an increase in the end-cap energy and accordingly to an increase in average micellar length. The decrease of E_{sciss} after the first maximum is related to the formation of branching points.[4] In that case, the scission energy is related to the average contour length between branching points $\bar{L}_c$, and an increase in the number of branching points will lead to a decrease in $\bar{L}_c$, which corresponds to a decrease of the scission energy. The second increase is again attributed to an increase of the micellar length $\bar{L}$, and this is in agreement with the cryo-TEM images showing a decrease of the branching density accompanied by an increase of micellar length. And finally, the decrease of E_{sciss} after the second maximum can be rationalized in terms of a shortening of the micelles and an increase of the branching density as again confirmed by cryo-TEM images. In conclusion, the variation of E_{sciss} directly shows changes in micellar structure induced by the variation of ionic strength, and the results are qualitatively in line with the cryo-TEM study on the same salt/surfactant system performed at lower surfactant concentration.[4] Finally, it should be noted that the DWS absolute values of E_{sciss} are about a factor 2 higher compared to the mechanical data. The reason for this shift is due to deviations in the Gmin″ DWS data, especially at temperatures of 20 and 25 °C where $G'' \ll G'$. Contrary to mechanical measurements, the in- and out-of-phase contributions are not measured independently in a DWS experiment but have to be extracted from a single value of the slope $\delta \ln\langle \Delta r^2(t)\rangle / \delta t$. As a consequence, if $G'(\omega)$ and $G''(\omega)$ are of different magnitude, the lower value extracted from DWS measurements is often not very well defined and here results in Gmin″ values much lower than that from mechanical measurements. Consequently, the mechanical measurements are more appropriate for a determination of absolute values of Esciss.

4.2.3. Persistence Length of Wormlike Micelles. The persistence length lp has been determined from the absolute value of G^* in the $\omega^{3/4}$-scaling regime according to eq 7. In order to obtain more reliable data in the ultrahigh frequency regime (up to 10^6 rad/s), we applied a simple (self-consistent) correction scheme to account for inertial effects when the motion of the tracer particles changes from Brownian to ballistic. The inset of Figure 6 shows the variations of G' and G'' as a function of frequency with and without inertial correction. In particular, G' is strongly modified by this correction and the unphysical downward curvature at frequencies $> 10^5$ rad/s is removed and G' follows the $\omega^{3/4}$-scaling analogous to G''. The inertia correction also modifies G'', and we have used this data set to calculate l_p, since the $\omega^{3/4}$-scaling is more evident and extends over a broader frequency range in G'' than in G'. We fit the function $G'' = k_{DWS}\omega^{3/4}$ to the experimental data and calculate l_p from the resulting k_{DWS} value according to eq 7.This equation requires a lateral drag coefficient $\delta = 4\pi\eta_s/\ln(0.6\lambda/d_{mic})$. The characteristic length λ is set equal to the mesh size, η_s is the solvent viscosity, and for the micelle diameter we insert $d_{mic} = 2.6$ nm.[39] This results in $\delta = 0.005$ N s/m^2. Figure 7 shows the variation of l_p as a function of salt concentration from DWS measurements. We observe a decrease of l_p from ∼30 to ∼26 nm over the total range of salt concentration investigated. Obviously, the linear-to-branched transition does not have a significant effect on l_p, and this increase in flexibility is considered to be an ionic strength effect due to the screening of electrostatic repulsion. In order to verify this assumption, we compared our results with the predictions of the OSF theory. According to this theory, for charged systems such as ordinary polyelectrolytes or wormlike micelles of ionic surfactants, the persistence length l_p can be expressed as a sum of an intrinsic component $l_{p,0}$ and an electrostatic component $l_{p,e}$:[58,59]

(58) Odijk, T. *J. Polym. Sci., Polym. Phys. Ed.* **1977**, *15*(3), 477–483.
(59) Skolnick, J.; Fixman, M. *Macromolecules* **1977**, *10*(5), 6717–6727.

$$l_p = l_{p,0} + l_{p,e} \tag{13a}$$

and the electrostatic contribution $l_{p,e}$ is given by

$$l_{p,e} = \frac{1}{4\kappa^2 l_B} \tag{13b}$$

with the Bjerrum length $l_B = 0.71$ nm and the Debye length κ^{-1} (nm) $= 0.304/(C_{salt})^{1/2}$.

This electrostatic contribution has been investigated in various surfactant/salt systems,[29,60−62] but in the majority of cases no systematic investigations have been performed comparing experimental results for l_p and predictions of OSF theory. Schurtenberger et al.[59] made such a comparison for the system composed of nonionic hexaethylene glycol mono-*n*-hexadecyl ether ($C_{16}E_6$) "doped" with a small amount of ionic surfactant 1-hexadecane sulfonic acid ($C_{16}SO_3Na$) in the presence of nonpenetrating counterion (NaCl). They found that $l_{p,e}$ absolute values were significantly higher than those predicted by the OSF theory, but they were not able to explain this systematic deviation. For the system investigated here, the variation of the persistence length l_p^{OSF} calculated from eq 13b is given in Figure 7. This electrostatic contribution is very small; l_p^{OSF} decreases by less than 1 nm in all the salt ranges investigated. Despite the experimental uncertainty of the l_p^{DWS} values, their decrease is significantly stronger than that predicted by OSF theory. Similar observations were obtained by Galvan-Miyoshi et al.[15] for the system CTAB/NaSal. Schubert et al.[11] also found a strong decrease of the persistence length with increasing salt for a mixed cationic/anionic micellar solution composed of cetyl trimethylammonium tosylate (CTAT) and sodium dodecyl benzyl sulfonate (SDBS) with added Na tosylate penetrating salt. The dependence on ionic strength follows the κ^{-2}-scaling predicted by OSF theory, but again the absolute values are much larger than expected by OSF theory. We assume that the increase in flexibility is due to the incorporation of more and more penetrating salicylate ions as R increases. Indeed, the penetration into the interior of the micelle by the salicylate ions can reverse the charge of the micelle from positive to negative, involving changes of dynamical properties, and can be responsible for the stronger increase in flexibility compared to the electrostatic contribution. In order to further elucidate this phenomenon, a similar study using a system with nonpenetrating counterions is in progress.

Finally, using our l_p^{DWS} experimental values, we calculated the contour length $\bar{L}$ of the micelles from the equations $(G\min''/G0) \approx (l_e/\bar{L})$ with $l_e \approx \xi^{5/3}/l_p^{2/3}$ and $\xi = (k_BT/G_0)^{1/3}$. Figure 8 shows the dependence of $\bar{L}$ as a function of R. $\bar{L}$ exhibits two maxima analogous to the scission energy, and this result confirms the findings on E_{sciss} in section 4.2.2 and demonstrates the consistency of our data analysis.

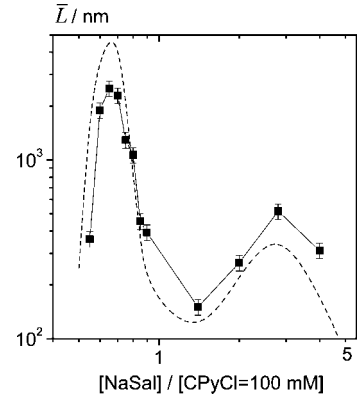

Figure 8. Dependence of the contour length $\bar{L}$ as a function of R obtained from DWS (squares). The dashed line represents the variation of the zero-shear viscosity η_0 in an arbitrary unit.

5. Conclusion

The system CPyCl/NaSal is known to exhibit two maxima in zero-shear viscosity as the salt concentration is varied.[2] The different viscosities are a result of structural changes as confirmed by cryo-TEM imaging.[4] At low salt concentration, the micelles are linear and their average contour length increases with increasing ionic strength. The first viscosity maximum corresponds to a transition from linear to branched micelles. The second viscosity increase corresponds to a decrease of the branching density accompanied by an increase of micelle length, and the second viscosity maximum to a shortening of the micelles with an increase of the branching density. With further increase of salt concentration, the formation of micellar rings is also observed. We have used various mechanical techniques as well as DWS optical microrheology to characterize the linear viscoelastic properties of this surfactant/salt system in a broad frequency range from 0.01 up to 10^6 s^{-1}. At a fixed surfactant concentration of 100 mM, we varied the salt/surfactant ratio R from 0.5 to 4. From these dynamic measurements, we can directly determine important structural features such as the cross-link density of the entanglement network, the scission energy, and the persistence length l_p. The persistence length l_p decreases monotonically with increasing salt concentration. This decrease is stronger than that predicted by the OSF theory which takes into account electrostatic screening effects. We attribute this to an additional increase in micellar flexibility due to the strongly binding salicylate counterion, which is known to penetrate into the micelles. This will be further investigated by a comparative study using a nonpenetrating counterion. The transition from linear to branched micelles obviously has no significant influence on l_p. The plateau modulus G_0 increases at the linear-to-branched micelles transition, and this is attributed to the additional contribution of branching points to the cross-link density. The scission energy E_{sciss} exhibits two maxima analogous the zero-shear viscosity, which can be understood in terms of the variation of micellar length and variation of the amount of branched micelles and contour length between branching points.

Acknowledgment. The authors thank D. Danino (Department of Biotechnology and Food Engineering, Technion, Haifa, Israel) for providing unpublished results of her cryo-TEM experiments and for fruitful discussions.

LA802323X

(60) Sommer, C.; Pedersen, J. S.; Egelhaaf, S. U.; Cannavacciuolo, L.; Kohlbrecher, J.; Schurtenberger, P. *Langmuir* **2002**, *18*, 2495–2505.

(61) Cannavacciuolo, J.; Pederson, S.; Schurtenberger, P. *Langmuir* **2002**, *18*, 2922–2932.

(62) Magid, L. J.; Han, Z.; Li, Z.; Butler, P. D. *J. Phys. Chem. B* **2000**, *104*(29), 6717–6727.